Isotherms and thermodynamics of malachite green on CO_2-activated carbon fibers

Joon Hyuk Lee
Hanyang University
Soon Hong Lee
Anyang University
Dong Hack Suh (dhsuh@hanyang.ac.kr)
Hanyang University

Short Report

Keywords: Malachite green, Activated carbon fibers, Carbon dioxide utilization, Isotherms, Thermodynamics, Adsorption

Posted Date: April 15th, 2021

DOI: https://doi.org/10.21203/rs.3.rs-424292/v1

Abstract

Carbonaceous adsorbents have received substantial attention in the past decades because of their porous surface characteristics. However, the majority use of strong acids for the surface modification and the subsequent surface decrease remains challenging. Here, we designed porous carbon fibers with the aid of CO_2 during activation for effective malachite green (MG) adsorption. The physiochemical mechanisms have been characterized both experimentally and numerically to decipher the underlying relevance of CO_2-activation on the MG adsorption capacity. The obtained samples are dominated by micropores, resulting in a high specific surface up to 1012 m^2 g^{-1} via 60 min of CO_2-activation. The adsorption isotherm was fitted to Langmuir with the maximum adsorption capacity of 555.56 mg L^{-1}. Thermodynamics revealed endothermic in nature and the spontaneous adsorption process. By using the primary culprit of global warming, this work advances the design of carbonaceous adsorbents for cationic dye removal. **(144/150)**

Introduction

Dyes are colorants that chemical structures predefine the impart color with some degree of permanence [1-2]. Synthetic organic dyes consist the largest portion of coloring substances and have attracted increasing interest over the last decade due to their indispensable role in printing, dyeing, battery manufacturing and textile industries [3-4]. Malachite green (MG) is a representative triphenylmethane cationic dye that can exist as dye salt, carbinol or pseudobase [5]. Due to its high soluble and stable characteristics in water, there is a large body of experimental evidence showing teratogenic, mutagenic and carcinogenic effects on human cells [6-7]. Moreover, the wastewater containing MG is considered to be one of the most challenging industrial wastewaters for purification [8]. Therefore, seeking an effective separation route has always been a longstanding objective of chemists. Several separation methods including ozonation, coagulation-flocculation, ion-exchange, photodegradation and advanced oxidation processes have been extensively studied to address the practical separation of MG. The aforementioned methods are yet hindered by complex manufacturing processes, high operational costs and additional harmful by-products [9]. Besides these approaches, adsorption is one widely adopted method for the purification of dye-containing industrial wastewater [10].

A number of carbonaceous materials such as activated carbon (AC), activated carbon fiber (ACF), graphene, graphene oxide and reduced graphene oxide are gaining immense interest owing to their porous structure and high adsorption capacity. The presence of ample adsorption sites and negatively charged oxygen-containing functional groups (-OH, -COOH, C-O/C=O) in carbonaceous materials may promote a favorable adsorption environment of cationic dyes [11-13]. ACs are known as porous carbonaceous material having irregularly shaped particles in powder or granular forms [14]. ACs have suitable features for the aimed application, however, adsorbate molecules have to pass macropores and mesopores first before entering micropores. ACFs are introduced to overcome deficiencies of ACs, since adsorbent molecules can be directly reached to micropores. It is worth underlining that ACF is also a low-

cost and easy-collectible adsorbent compared to graphene-based adsorbents. Despite all the advantages of ACFs, their use has been limited due to relatively low adsorption capacity. Hence, surface modification is of paramount importance for ACF-based adsorbents to compete with advanced carbonaceous materials. With untiring efforts, researchers have succeeded in preparing ACFs under strong acids to increase the number of oxygen-containing functional groups [15-16]. Although thus-prepared ACFs have experienced an inevitable decrease in surface areas, increased oxygen-containing functional groups have resulted in high adsorption capacity of heavy metals via the ion-exchange mechanism. Nevertheless, introducing strong acids may be insufficient in this case, because the MG adsorption capacity can be hampered by an acidic environment [17].

Here, we report an industrially applicable MG adsorption technique using CO_2-ACFs. We highlight that the primary culprit of global warming is an essential driving force for achieving high surface characteristics of ACFs, verified by experimental evidence and theoretic calculations. A fairly low oxygen-containing functional groups were introduced during CO_2 activation. A significant advantage here of using CO_2 is in the greater adsorption capacity of MG without any surface decrease, which is not possible with pre-defined surface modification techniques. The pore-growth phenomenon is further demonstrated via CO_2-surface reaction. With these features in hand, CO_2-ACF absorbents may lead to new opportunities in wastewater separation of synthetic organic dyes with cationic molecules.

Experimental

Preparation of samples

ACFs were prepared from stabilized pitch fibers. A principal goal in developing pitch fibers is to convert isotropic pitches to mesophase upon designated treatments [18]. The key fabrication steps are as follows; stabilization, carbonization and activation (also overviewed in Fig. 1(a)). First, 100 mg of precursors were stabilized in a horizontal reaction tube via air mood (2 L min^{-1}) of 300 °C for 3 hr. Oxidative stabilization of precursors allows crosslinking of aromatic molecules (Fig. 1(b)). Subsequently, samples were carbonized under N_2 gas (2 L min^{-1}) and heated to the target temperature of 800 °C. The high temperature in the absence of air and the presence of N_2 gas removes the unnecessary impurities from a carbonaceous substrate [19]. However, vigorous heat treatment during carbonization may leave disorganized carbon. Activation reorganizes the carbon and enhances the pore distribution. Once the temperature has reached the suggested temperature, activation was done by adding CO_2 gas instead of N_2 gas for 20, 40 and 60 min, respectively. ACFs with various CO_2-activation times were further denoted as ACF-2, ACF-4 and ACF-6 for convenience. Morphologies were analyzed using scanning electron microscopy (XL30, PHILIPS) coupled with element energy dispersive spectroscopy (APPOLO40, AMETEK) prior to the following experiments. The roughness and the circular pores gradually emerged as the CO_2-activation time increased (Fig. 1(c)). Depending on the nature of samples, the detected C field was in the order of ACF-2 > ACF-4 > ACF-6 (Fig. 1(d)). Such decrease may due to the increase of oxygen-containing functional groups within newly developed micropores. The above observations highlight the possibility of

CO_2-based surface modification, where one may expect favorable surface characteristics via additional pore-growth.

Surface characteristics

Samples were washed with de-ionized water and heated at 300 °C for 24 hr under a vacuum state of 1.33×10^{-3} Pa (VacPrep 061, Micromeritics). Thereafter, surface characteristics were investigated by BET-BJH measurement (ASAP 2020, Micromeritics) [20]. X-ray photoelectron spectra was employed with an equipped Al Kα source at 10^{-9} Torr (Sigma Probe, Thermo VG Scientific). Fitted curves were used to analyze the surface composition.

Isotherms and thermodynamics

The solution of MG before and after adsorption was analyzed via inductively coupled plasma-optical emission spectrometry (Optima 5300DV, PerkinElmer). NaOH and HCl solutions of 0.1 M each were used to adjust pH to the designated value. Two parameter models of Langmuir and Freundlich were chosen to correlate the experimental adsorption isotherms of MG. The changes in Gibbs free energy (ΔG^0), enthalpy (ΔH^0) and entropy (ΔS^0) for the adsorption process were confirmed to observe the adsorption thermodynamics. Further theoretical details are described in relevant studies [21-22].

Results And Discussion

All samples showed similar porous characteristics of dominant micropores over external pores. Specific surface and yield of samples are found to be in a reversible-correlation (Figs. 2(a)-2(c)). Specific surface of samples was in the order of ACF-6 (1012 $m^2\ g^{-1}$) > ACF-4 (933 $m^2\ g^{-1}$) > ACF-2 (841 $m^2\ g^{-1}$). From the data set, it is evident that CO_2-activation time promotes pore growth. ACF-6 exhibited 23.15% and 10.85% more micropores and 25.85% and 14.84% less external pores compared to ACF-2 and ACF-4, respectively. A visible decrease in the yield is due to the diffused CO_2 during activation, which introduces CO. Some portions of CO may react with partial O atoms and reform additional CO_2. By enduring high activation temperature, these dissociated products of CO_2 enlarge pores and result in an overall decrease of yield. These results indicate that the maturity of pores can be achieved from the sacrificial reduction of yield. This is in consistent with the observation of the C content in ACF-6 (Figs. 2(d) and 2(f)). The binding energy of C-C depends on the degree of disorder of carbonaceous materials [23]. It is clear that the aforementioned ratio for ACF-6 is larger than the other two, indicating great crosslinking of pitch fractions. The O content is due to the oxygen-containing functional groups, whereas a high number of pores enables more room for the distribution of oxygen-containing functional groups (Fig. 2(g)). The majority of N content, however, remained at approximately 0.04 – 0.05%. We note that the existence of N content reflects its amount in the starting material (Fig. 2(e)).

The adsorption of MG onto a fixed sample amount of 0.05 g was studied by varying the surrounding environment. As shown above, the adsorption process is believed to be driven via the high numbers of

negatively charged oxygen-containing functional groups, as well as micropores on the surface. The time required to reach the adsorption equilibrium increased from 2 to 4 hr for the initial concentrations of MG from 50 to 150 mg L^{-1}, respectively (Fig. 3(a)-left). A high concentration of MG enables overcoming the resistance to mass transfer between the aqueous and solid phases. At the same initial MG concentration of 150 mg L^{-1}, the adsorption capacity slightly increased with the corresponding temperature from 25 to 45 °C (Fig. 3(a)-right). This confirms the endothermic nature of the adsorption process, whereas the MG molecules can preferably interact with the active sites on the sample surface. The adsorption capacity of MG could be further accelerated by increasing the initial pH from 2 to 10 (Fig. 3(b)). With a higher initial pH, an increase in positive charges on the surface sites can be expected. This trend further leads to an enhanced electrostatic force toward positively charged MG cations and smoothens the peak from pH 6. Meanwhile, a decrease in adsorption capacity at low initial pH below 4 is due to an electrostatic repulsive force. These results align well with the CO_2-activation time and establish an applicable direction to improve the adsorption capacity of MG (Fig. 3(c)). At a constant sample amount with various MG concentrations from 50 to 150 mg L^{-1}, the Langmuir isotherm showed more reliable R^2 values in the range of 0.9900 - 0.9921 than those of the Freundlich isotherm in the range of 0.9807 - 0.9898 (Figs. 3(d)-(e)). This indicates that the adsorption has occurred with the formation of a monolayer and also confirms the chemisorption [24]. The maximum adsorption capacity for MG was in the order of ACF-6 (555.56 mg L^{-1}) > ACF-4 (526.32 mg L^{-1}) > ACF-2 (454.55 mg L^{-1}), respectively, which is in good agreement with the above trend. Thermodynamic parameters were estimated using equilibrium constants as a function of temperature in the range of 25 – 45 °C (Figs. 3(f)-(g)). The adsorption of MG was endothermic in nature as indicated by the positive values of ΔH^0 and ΔS^0. The negative values of ΔG^0 signify the spontaneous adsorption process and this could be further increased at the higher temperature.

Conclusion

In summary, we have prepared a microporous ACF via CO_2-activation for the highly efficient removal of MG. Combined experimental and mathematical investigations demonstrate that the high adsorption capacity could be effectively achieved by employing 60 min of CO_2 during activation. The highest adsorption capacity (146.93 mg L^{-1}) occurred at 45 °C and 150 mg L^{-1} of MG concentration. Langmuir isotherm provided the best fitting of the experimental data with the maximum adsorption capacity of 555.56 mg L^{-1}. The measured changes of enthalpy and entropy against temperature resulted in positive values, indicating endothermic in nature. The negative values of free energy informed the spontaneous adsorption process. The foregoing results may open up a practical approach for the rational design of highly efficient adsorbent materials for cationic dye removal under the concept of green chemistry.

Declarations

Declaration of interests

The authors declare that they have no known competing financial interests or personal relationships that could have appeared to influence the work reported in this paper.

Funding sources

This research did not receive any specific grant from funding agents in the public, commercial, or not-for-profit sectors.

References

1. N.P. Raval, P.U. Shah, N.K. Shah, Appl. Water. Sci. 7(7) (2017) 3407-3445. https://doi.org/10.1007/s13201-016-0512-2
2. A. Tkaczyk, K. Mitrowska, A. Posyniak, Sci. Total. Environ. 717 (2020) 137222. https://doi.org/10.1016/j.scitotenv.2020.137222
3. K. He, G. Chen, G. Zeng, A. Chen, Z. Huang, J. Shi, L. Hu, Appl. Catal. B. 228 (2018) 19-28. https://doi.org/10.1016/j.apcatb.2018.01.061
4. J. Yang, Y. Yang, A. Li, Z. Wang, H. Wang, D. Yu, L. Guo, Energy. Storage. Mater. 17 (2019) 334-340. https://doi.org/10.1016/j.ensm.2018.06.030
5. S. Srivastava, R. Sinha, D. Roy, Aquat. Toxicol. 66(3) (2004) 319-329. https://doi.org/10.1016/j.aquatox.2003.09.008
6. M. Mobarak, E.A. Mohamed, A.Q. Selim, M.F. Eissa, M.K. Seliem, J. Mol. Liq. 273 (2019) 68-82. https://doi.org/10.1016/j.molliq.2018.09.132
7. T.K. Vo, T.P. Trinh, V.C. Nguyen, J. Kim, J. Ind. Eng. Chem. 95 (2021) 224-234. https://doi.org/10.1016/j.jiec.2020.12.023
8. Y. Zhuang, F. Yu, H. Chen, J. Zheng, J. Ma, J. Chen, J. Mater. Chem. A. 4(28) (2016) 10885-10892. https://doi.org/10.1039/C6TA02738E
9. M.A. Adebayo, J.I. Adebomi, T.O. Abe, F.I. Areo, Colloids. Interface. Sci. Commun. 38 (2020) 100311. https://doi.org/10.1016/j.colcom.2020.100311
10. M.C. Ribas, M.A. De Franco, M.A. Adebayo, E.C. Lima, G.M. Parkes, L.A. Feris, Appl. Water. Sci. 10(6) (2020) 154. https://doi.org/10.1007/s13201-020-01237-9
11. C.M. Park, J. Han, K.H. Chu, Y.A. Al-Hamadani, N. Her, J. Heo, Y. Yoon, J. Ind. Eng. Chem. 48 (2017) 186-193. https://doi.org/10.1016/j.jiec.2016.12.038
12. K. Gupta, O.P. Khatri, J. Colloid. Interface. Sci. 501 (2017) 11-21. https://doi.org/10.1016/j.jcis.2017.04.035
13. A.S. Eltaweil, H.A. Mohamed, E.M. Abd El-Monaem, G.M. El-Subruiti, Powder. Technol. 31(3) (2020) 1253-1263. https://doi.org/10.1016/j.apt.2020.01.005
14. R. Khosravi, A. Azizi, R. Ghaedrahmati, V.K. Gupta, S. Agarwal, J. Ind. Eng. Chem. 54 (2017) 464-471. https://doi.org/10.1016/j.jiec.2017.06.036

15. T. Wu, G. Wang, Q. Dong, B. Qian, Y. Meng, J. Qiu, Electrochim. Acta. 176 (2015) 426-433. https://doi.org/10.1016/j.electacta.2015.07.037
16. J. Yu, C. Chi, B. Zhu, K. Qiao, X. Cai, Y. Cheng, S. Yan, Sci. Total. Environ. 700 (2020) 134412. https://doi.org/10.1016/j.scitotenv.2019.134412
17. W. Qu, T. Yuan, G. Yin, S. Xu, Q. Zhang, H. Su, Fuel. 249 (2019) 45-53. https://doi.org/10.1016/j.fuel.2019.03.058
18. Z.W. Liang, Y.G. Lu, Z.L. Sun, H. Luo, New. Carbon. Mater. 35(5) (2020) 591-598. https://doi.org/10.1016/S1872-5805(20)60512-1
19. M.F. Hassan, M.A. Sabri, H. Fazal, A. Hafeez, N. Shezad, M. Hussain, J. Anal. Appl. Pyrolysis. 145 (2020) 104715. https://doi.org/10.1016/j.jaap.2019.104715
20. J.H. Lee, S.H. Lee, D.H. Suh, J. CO2. Util. 39 (2020) 101163. https://doi.org/10.1016/j.jcou.2020.101163
21. M. El Haddad, A. Regti, R. Slimani, S. Lazar, J. Ind. Eng. Chem. 20(2) (2014) 717-724. https://doi.org/10.1016/j.jiec.2013.05.038
22. T. Kameda, R. Honda, S. Kumagai, Y. Saito, T. Yoshioka, Mater. Chem. Phys. 236 (2019) 121784. https://doi.org/10.1016/j.matchemphys.2019.121784
23. J.S. Lee, Y.K. Kim, J.Y. Hwang, H.I. Joh, C.R. Park, S. Lee, Carbon. 121 (2017) 479-489. https://doi.org/10.1016/j.carbon.2017.06.010
24. T. Kameda, R. Honda, S. Kumagai, Y. Saito, T. Yoshioka, J. Solid. State. Chem. 277 (2019) 143-148. https://doi.org/10.1016/j.jssc.2019.06.002

Figures

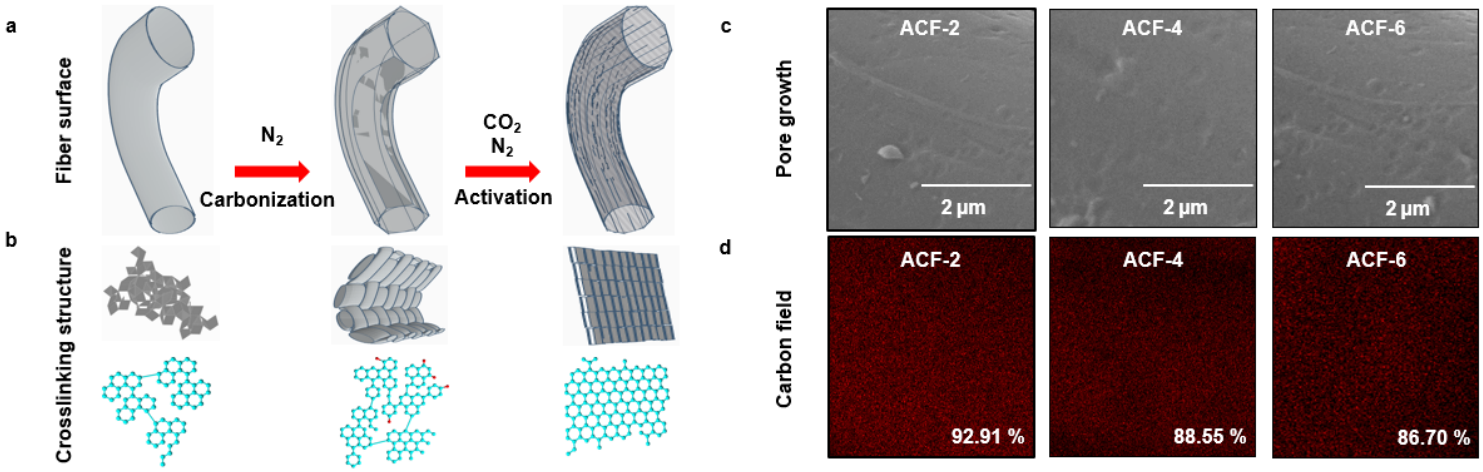

Figure 1

Schematic illustration of (a) possible fiber structures and their (b) corresponding crosslinking structures during carbonization and activation. Pore growth by various CO2-activation times is scanned (c) under

the operating acceleration voltage of 2.00 kV. The C field is colored red as can be seen in (d), while other possible O and N contents black.

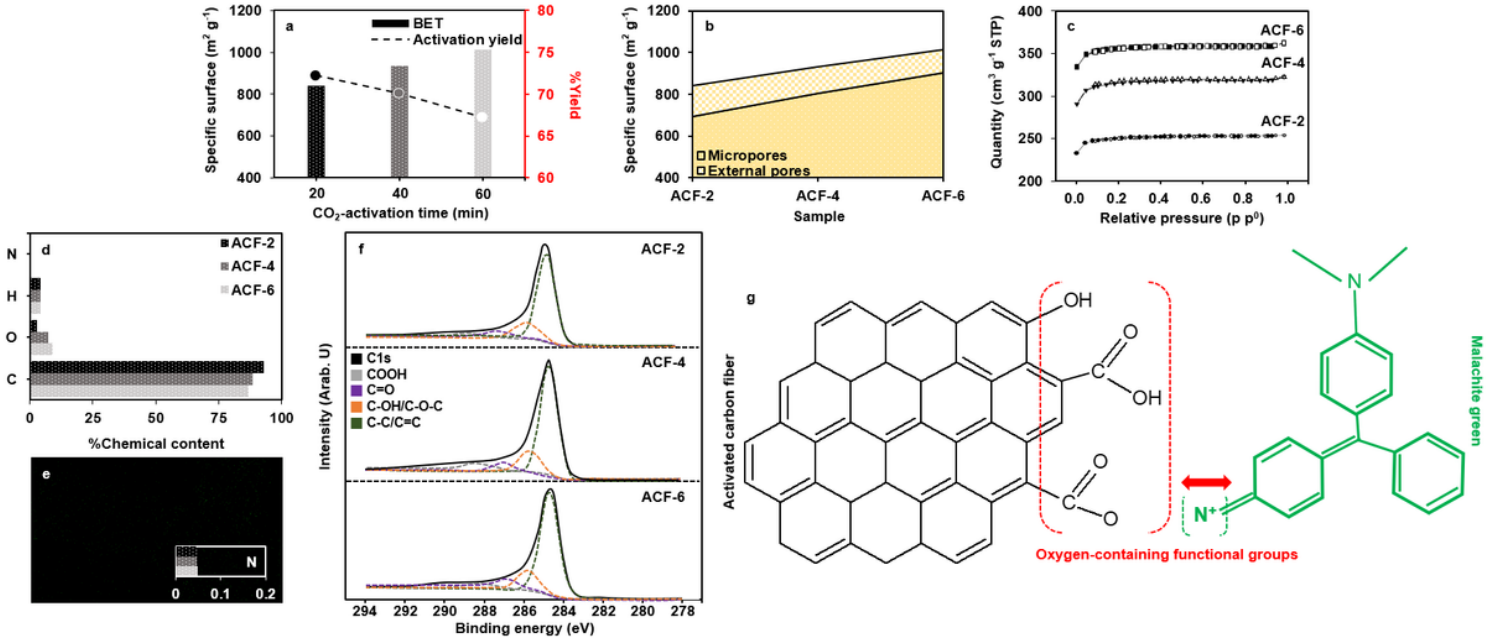

Figure 2

Specific surface and yield of samples as revealed by a function of CO2-activation time are plotted in (a). The following structure parameters including micropores and external pores are illustrated in (b). N2 adsorption-desorption isotherm of samples is plotted in (c). Primary chemical contents are shown in (d). The O content was calculated by subtracting the sum of C, H and N contents from the total amount. Given that the N content consists of approximately 0.04 – 0.05%, the N field is colored blue as can be nearly seen in (e). Herein, the N field is obtained from ACF-6. The inset shows the chemical content of N. X-ray photoelectron spectra of deconvoluted C1s are plotted in (f) to observe pitch fractions and oxygen-containing functional groups. A simplified mechanism for the possible interaction between oxygen-containing functional groups and MG is visualized in (g).

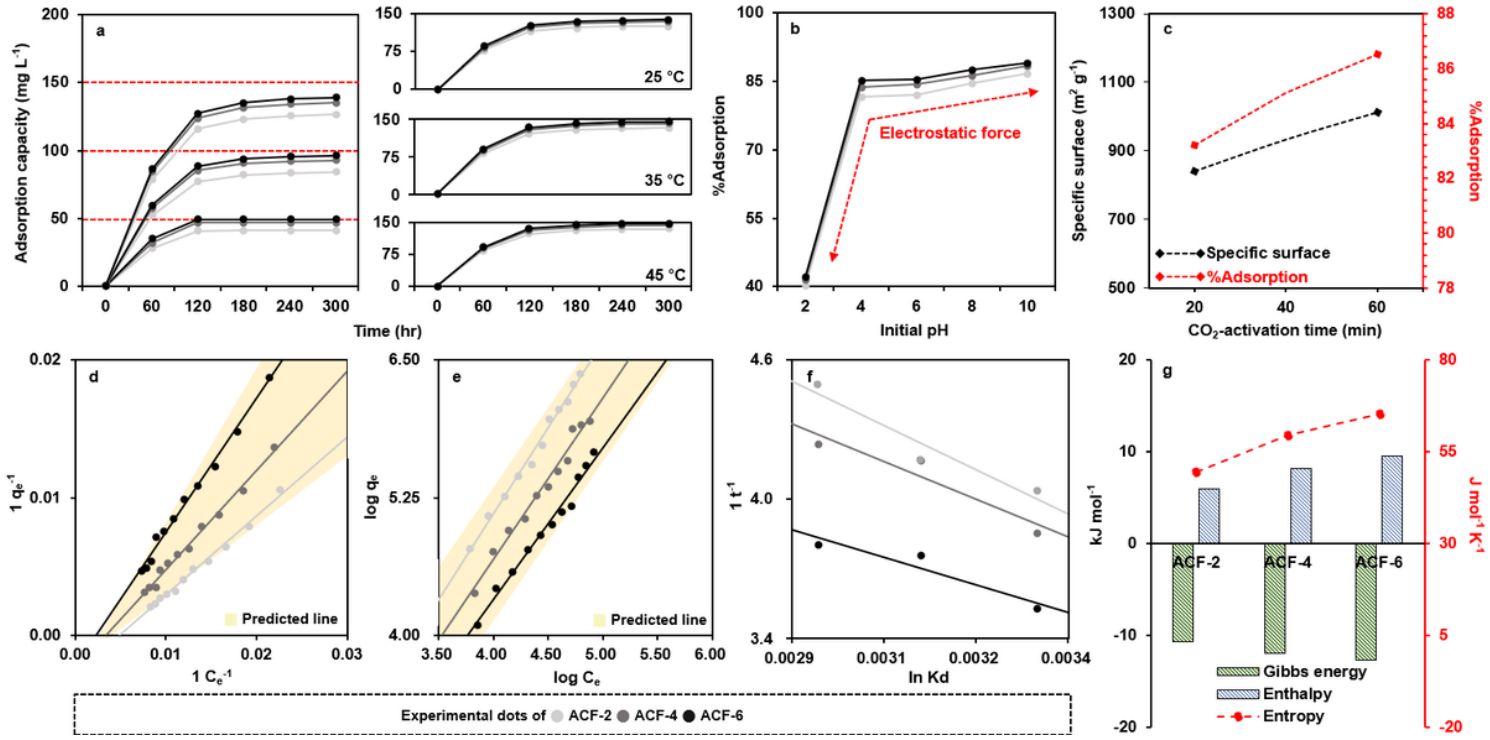

Figure 3

The effect of the initial concentration (left) and temperature (right) on the adsorption capacity of MG by designated time frame is depicted in (a). The effect of the initial pH of MG solution on the adsorption capacity is illustrated in (b). An experimental comparison of the adsorption capacity of MG calculated with different specific surfaces is plotted in (c). Langmuir and Freundlich isotherm models for MG adsorption at various initial concentrations are plotted in (d) and (e). The effect of temperature on the MG adsorption and the corresponding thermodynamics are presented in (f) and (g).